Characterization of Cellulose Nanocrystal Suspension Rheological Properties Using a Rotational Viscometer

Yucheng Peng
Changlei Xia
Brian Via

Abstract

Interest in cellulose nanocrystal (CNC) recently has been growing significantly. Many applications have been developed for CNC and appropriate procedures to handle the CNC suspensions are critical for these applications. In this study, we explored a method evaluating CNC suspensions based on rheological property characterization. We used a rotational viscometer to characterize CNC suspensions at concentrations of 3, 4, 5, and 6 wt.%. We collected primary readings from the rotational viscometer, including spindle rotation speed and torque, to generate apparent viscosity and shear rate for CNC suspensions. We applied three different methods summarized from the literature to calculate apparent viscosity and real shear rate. We critically analyzed differences among calculation results from the three methods. Shearing thinning behaviors obeyed the power law flow model for all CNC suspensions in the shear rate tested. At different concentrations, consistency and flow behavior indices in the model differed in the measured shear rate range. With the same shear rate, higher concentration CNC suspension had a higher apparent viscosity. The apparent viscosity of the CNC suspension was associated with its weight concentration in a power law relationship. This study indicated that a rotational viscometer can be used as a quality control tool for characterizing the rheological properties of the CNC suspensions. We made recommendations for using appropriate calculation methods to obtain shear rate and apparent viscosity of CNC suspensions from the primary readings of a rotational viscometer under different situations.

Cellulose nanocrystals (CNCs) are nanosized cellulose particles in rod or spindle shapes and are made from cellulose materials in different formats and from a variety of sources, including wood, plants, marine animals, algae, and bacteria (Rånby 1951, Eichhorn et al. 2010, Habibi et al. 2010, Chen et al. 2015). CNCs have recently received a substantial amount of interest in different industrial sectors because of their unique characteristics, including renewability, high aspect ratio, high mechanical properties, transparency, large surface area and modifiable surface, and light weight (Peng et al. 2012, Li et al. 2015). Their growing importance is demonstrated by the increasing number of publications about CNCs during recent years. A search of ''cellulose nanocrystal'' in ISI Web of Knowledge in January 2021 showed that publications per year related to the topic of CNC increased from 2 in 2002 to >300 in 2020 (Fig. 1).

CNCs generally are obtained through acid hydrolysis of cellulose materials via digestion of the amorphous phases, generating rigid materials with high crystallinities (Aulin et al. 2009, Habibi et al. 2010, Chen et al. 2015). After production, either negatively or positively charged CNC particles are obtained through surface modifications, dispersing themselves in water and retaining their nanoscale dimensions as a result of electrostatic repulsion forces (Rånby 1951, Revol et al. 1992, Araki et al. 1998, Peng et al. 2012). Many different applications have been developed
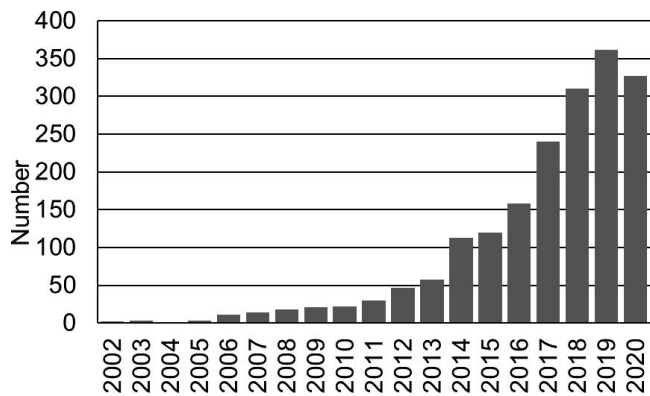
Figure 1.—Number of publications related to cellulose nano-crystal in each year (derived from search for "cellulose nanocrystal" in ISI Web of Knowledge, January 2021).

since the discovery of CNC particles and handling CNC suspensions is a crucial step for all these applications, which then need further treatments. The rheological behaviors of CNC suspensions play a critical role in these processes and can have important consequences regarding the final applications (Yasuda et al. 2004, Hubbe et al. 2017). Additionally, the basic material handling processes—including CNC suspension production, transportation, storage, pumping, mixing, and metering—all require viscosity data as a basic parameter for an accurate operation (Hubbe et al. 2017, Lindström 2017). This is especially important when handling high-value nanoscale material of CNC. The rheology of CNC suspensions has been intensively and comprehensively studied using high-end technologies of the rheometer, and a wide range of shear rates and detailed modeling of rheological data have also been provided in the literature (Araki et al. 1998, Bercea and Navard 2000, Urena-Benavides et al. 2011, Shafiei-Sabet et al. 2012, Li et al. 2015, Hubbe et al. 2017, Moberg et al. 2017, Buffa et al. 2019, Liao et al. 2020). However, the research community has not offered a practical and convenient apparent viscosity measurement for CNC suspensions as a quality control methodology. Simultaneously, the wide variety of CNC samples from different sources, manufacturing processes, and facilities complicate the details of rheological data characterization using a rheometer (Bercea and Navard 2000, Urena-Benavides et al. 2011, Shafiei-Sabet et al. 2012, Buffa et al. 2019, Liao et al. 2020). Development of a practical and convenient apparent viscosity characterization method would be a significant contribution to facilitate industrial applications of CNC materials.

The objective of this study is to develop a potential quality-control methodology for the research and development community that use CNC suspensions in their facilities, based on characterizing the viscosities of CNC suspensions using a rotational viscometer. A rotational viscometer is a powerful tool that is standard in facilities handling solutions, emulsions, suspensions, and slurries. The low cost and convenience of operation make it a very handy tool for laboratory research and development. A rotational viscometer can also provide data on the apparent viscosity of liquids, which are sensitive to property changes affected by particle sizes and shapes, particle agglomera-

tions and interactions, electrical charges, concentrations, etc. (Brookfield Engineering Laboratories 2017).

A rotational viscometer commonly rotates a cylindrical or a disk spindle of different sizes in a concentric container of fluid (Krieger 1968, Haŭgen and Tung 1976, Yang and Krieger 1978, Sikdar and Oré 1979, Williams 1979). The size of spindle or liquid holding cup determine the range of viscosities to be characterized. Temperature can also be controlled if needed during measurement. During operation, the spindle is rotated at a constant angular velocity and concomitant torque on the spindle is measured. The primary data generated through the measurement are spindle rotation speed (revolution per minute [RPM]) and torque. Depending on the liquid viscosity range, many data points can be obtained using one spindle rotating at different speeds. Compared with high-end technology measuring rheological property of suspensions via a rheometer, a rotational viscometer has limited range of shear rate. Another concern when using a rotational viscometer is the difficulty of interpreting data obtained from experiments for non-Newtonian liquids. Measurement of apparent viscosity of Newtonian fluids is straightforward using a rotational viscometer, and the same apparent viscosity can be obtained under different shear rates by changing spindle rotation speed (i.e., the angular velocity [Sikdar and Oré 1979, Williams 1979]). The linear velocity of the liquid between the spindle and the liquid holding cup under the shear flow caused by the rotation of the spindle changes linearly with distance from the spindle axis (i.e., the velocity gradient [shear rate] is constant). Maximum linear velocity of the liquid is located on the side of the spindle and zero liquid velocity is assumed on the side of the liquid holding cup. For non-Newtonian fluids, the linear velocity of the liquid between the spindle surface and the liquid holding cup changes nonlinearly with distance from the spindle axis. The shear rate of the liquid is a complex function of distance and cannot be analytically solved (Krieger and Maron 1952), and the real shear rate would remain unknown at any location of the liquid. Therefore, the apparent viscosity of non-Newtonian liquid would change as the shear rate changed and the real viscosity data would not be available from the measurement. CNC suspension is such a non-Newtonian liquid because high-aspect-ratio CNC particles in rod shapes are embedded in a Newtonian liquid (Jeffrey and Andreas 1976, Powell 1991, Mueller et al. 2009, Shafiei-Sabet et al. 2012, Hubbe et al. 2017, Moberg et al. 2017). For the same reason, multiple data points must be obtained during the measurement using a rotational viscometer to better understand the nonlinear flow of a non-Newtonian liquid.

Spindle rotation speed (RPM) and spindle torque can be read directly from a commercial rotational viscometer, and a preprogramed calculation procedure is used to calculate apparent viscosity. A specified constant is always used in the calculation of apparent viscosity and shear rate (Brookfield Engineering Laboratories 2017); however, many researchers have shown confusion when trying to generate the relationship between apparent viscosity and shear rate from this powerful tool for non-Newtonian liquids. The mechanism by which such viscosity data can be generated is not well-understood by the research community or industrial research laboratory personnel, and clarification of the calculation process is needed. Additionally, the real shear rate and apparent viscosity of the liquid
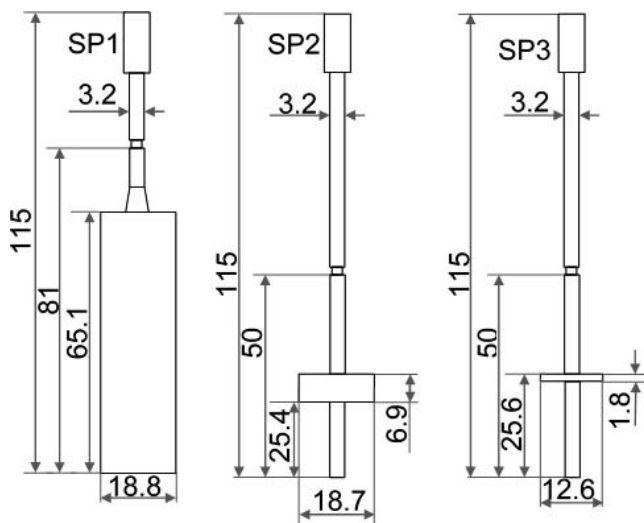
Figure 2.—The specifics (millimeters) of the spindles used in the viscosity measurement (as reported by the equipment supplier).

during measurement using a rotational viscometer is needed because no direct analytical solution has been demonstrated for non-Newtonian liquids (Krieger and Maron 1952, Krieger 1968, Yang and Krieger 1978). Several approximation methods have been proposed by different research groups and each method has been used in the literature for characterizing different fluids (Krieger and Maron 1952, Mitschka 1982, Rosen 1972, Brookfield Engineering Laboratories 2017).

In this study, we summarized three methods of treating the primary readings from a rotational viscometer measurement to obtain the relationship between the apparent viscosity and shear rate for non-Newtonian liquids and applied them to the CNC suspensions at four different concentrations: 3, 4, 5, and 6 wt.%. We hope this could help to clarify the advantages of each different shear rate and viscosity calculation method to the research community. We directly compared the three different methods and discuss differences among them. We generated the relationship between apparent viscosity and shear rate for the CNC suspensions, and also evaluated effect of CNC concentration on the suspension apparent viscosity.

Materials and Methods

Materials

We purchased CNC suspension at 6 wt.% from CelluForce (Montreal, Canada). The CNC was obtained from sulfuric acid hydrolysis of wood pulp followed by neutralization with sodium hydroxide. CNC suspensions at 5, 4, and 3 wt.% were prepared by diluting 6 wt.% CNC suspension with deionized water using a magnetic stirrer mixing at 870 RPM for 1 hour.

Methods

Apparent viscosity measurements reported in this work were made with an IKA Rotavisc lo-vi viscometer with its spindles SP1, SP2, and SP3 rotating in a 600-mL low form beaker at room temperature (22°C) with a spindle guard leg.

The specific dimensions as reported by the equipment supplier for spindles SP1, SP2, and SP3 are shown in Figure 2. This viscometer had continuous rotation speed ranging from 0 to 200 RPM. The inner diameter of the beaker holding the CNC suspension was 8.45 cm. Measurement temperatures were recorded by the viscometer and were observed to change within ≤1°C between different measurements. Prior to each viscosity measurement, we stirred the suspension of CNC at 870 RPM in the beaker for 1 hour using a magnetic stirrer, after which we let the suspension sit at room temperature overnight. During the viscosity measurement, we used spindle SP1 for CNC suspensions of 3, 4, 5, and 6 wt.%, and we used spindles SP2 and SP3 for CNC suspensions of 5 and 6 wt.%. The viscosities of CNC suspensions of 3 and 4 wt.% were out of range of the measurement capability of spindles SP2 and SP3. We controlled spindle rotation speeds during viscosity measurement with torque readings located between 10% and 90% of the full-scale torque, which is 673.7 dyne-cm. The primary readings generated during the viscosity measurement were spindle RPM, torque percentage (M%), and apparent viscosity (η). We recorded torque and apparent viscosity readings when the measurement system stabilized, and it took from approximately 30 seconds to 1 minute to obtain one data point. We used many spindle rotation speeds for each CNC suspension in the specified torque range (10% to 90%) to obtain as complete a rheological curve as possible within the capability of this viscometer.

Results and Discussion

Figure 3 shows plots of torque readings (%) M against spindle RPM, the primary readings from the rotational viscometer, for CNC suspensions at 3, 4, 5, and 6 wt.% using spindle SP1. Many data points were recorded for each suspension and a continuous curve can be formed within the testing torque range. For different concentrations of CNC, the same spindle rotation speeds generated different torques, resulting in different shear rate measurement ranges for the CNC suspensions. For each set of data, a trend line easily can be established in a power law relationship with a high coefficient of determination (R^2). The trend line equations and coefficient of determination for the relationship between spindle torque and rotation speed are also shown in Figure 3 for all the CNC suspensions. With the same spindle rotating at the same speed, a higher concentration of CNC suspension applied greater shear stress to the spindle, resulting in a greater torque.

Shear stress (τ) on the spindle surface applied by the CNC suspension during rotation can be calculated using equation (1) (Krieger and Maron 1952, Krieger and Elrod 1953, Brookfield Engineering Laboratories 2017):

$$\tau = \frac{673.7M}{200\pi r^2 L} \tag{1}$$

where r is the radius of spindle SP1 and L is the effective length of the spindle (Brookfield Engineering Laboratories 2017). Equation (1) only applies to spindle SP1, which has r and L of 0.942 cm and 7.493 cm, respectively. The effective length of 7.493 cm is used instead of the actual length of the spindle in order to compensate for the end effect of the spindle. Equation (1) shows that the shear stress is proportional to the torque reading, which indicates that shear stress applied by the CNC suspension to the spindle
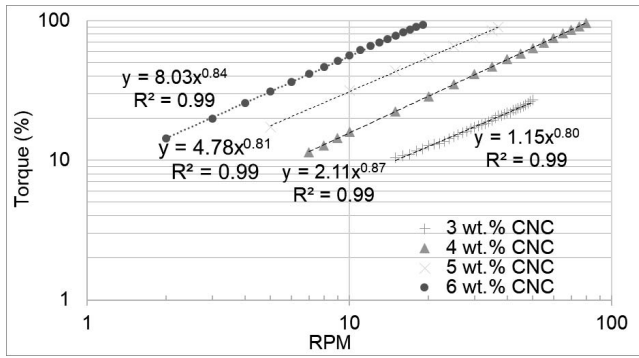
Figure 3.—The relationship between the torque reading and spindle revolutions per minute (RPM) for the CNC suspensions.

Figure 4.—The relationship between the apparent viscosity and the shear rate for the CNC suspensions calculated from Method 1.

surface is in a power law relationship with respect to the spindle RPM, which is directly related to the angular velocity of the spindle (radian per second) through equation (2):

$$\omega = \frac{2\pi}{60} N \qquad (2)$$

where N is the spindle rotation speed (RPM). With known angular velocity, the shear rate ($\dot{\gamma}$, sec^{-1}) at the spindle surface can be calculated using equation (3) (Brookfield Engineering Laboratories 2017):

$$\dot{\gamma} = \frac{2\omega(D/2)^2}{(D/2)^2 - r^2} \qquad (3)$$

where D is the inner radius of the CNC suspension holding cup (8.45 cm). This approximate shear rate calculation assumes that there was no wall slip between the CNC suspension and the surface of the spindle (i.e., the very thin layer of CNC suspension attached to the spindle surface rotated at the same speed as the spindle surface). At the same time, the shear rate calculated using equation (3) assumes that the liquid is Newtonian (Krieger and Elrod 1953, Krieger 1968, Haŭgen and Tung 1976). In addition, shear rate function as a distance from the center of the spindle can be represented in equation (4) below:

$$\dot{\gamma} = dv/dx = \frac{2\omega(D/2)^2 r^2}{x^2\left[(D/2)^2 - r^2\right]} \qquad (4)$$

where dv/dx is the velocity gradient, which is a derivative of the linear velocity of the liquid rotating with an angular velocity ω to the distance x from the center the spindle, and x is the distance at which the shear rate is being calculated ($r \leq x \leq D$). At the surface of the spindle, x equals r and equation (3) was obtained.

Combining equations (1), (2), and (3), apparent viscosity of the CNC suspension in centipoise ($cP = $ mPa·s) can be calculated using equation (5) below:

$$\eta = \frac{\tau}{\dot{\gamma}} = \frac{5052.75\left[(D/2)^2 - r^2\right]}{\pi^2 L (D/2)^2 r^2} \frac{M}{N} = C\frac{M}{N} \qquad (5)$$

where C is a constant related to the dimensions of the spindle and the liquid holding cup. It can be seen from equation (5) that the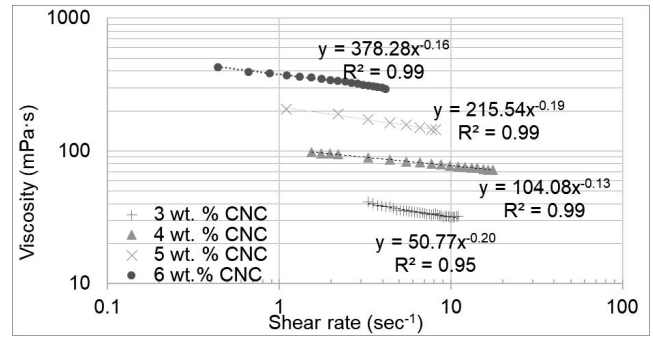 apparent viscosity calculated using this method can be directly derived from the relationship between the torque reading and the spindle rotating speed. With the dimensions of r, L, and D replaced by 0.942 cm, 7.493 cm, and 8.45 cm (Brookfield Engineering Laboratories 2017), the constant C can be calculated as 73, which is close to the number (72) suggested in the viscometer manual without a guard leg during the measurement. With the guard leg installed during the measurement, C is corrected to be 60 (Brookfield Engineering Laboratories 2017) and the apparent viscosity (mPa·s) during the measurement is calculated as

$$\eta = 60\frac{M}{N} \qquad (6)$$

The results showing the apparent viscosity calculated from equation (6) and the shear rate calculated from equation (3) are presented in Figure 4. Non-Newtonian fluids with shear thinning phenomena were observed for all the CNC suspensions. The higher concentration CNC suspension has a higher apparent viscosity. The empirical power law flow model (also called the Oswald De Waele model) can be used to fit the data in the shear rate range tested in this study (Fig. 4). The power law flow model is expressed as

$$\eta = k\dot{\gamma}^{n-1} \qquad (7)$$

where k is the consistency index and n is the flow behavior index. It can be seen from Figure 4 that different concentrations of CNC suspensions have different consistency and flow behavior indices. The consistency indices of the CNC suspensions decreased with decreasing concentrations and no trend was observed for the flow behavior indices. A similar power law relationship can be observed for apparent viscosity and spindle rotation speed (Fig. 5). The consistency indices for the CNC suspensions obtained from the plot of apparent viscosity against RPM are different from those obtained from apparent viscosity versus shear rate, whereas the flow behavior indices are all the same.

We designated the apparent viscosity and shear rate calculation method using equations (3), (5), and (6) as Method 1 in this study, and it comes along with the equipment. The primary apparent viscosity readings from the viscometer are based on the equation (5) calculation using spindle SP1 with a guard leg, and it works for a Newtonian liquid. However, the testing results for CNC
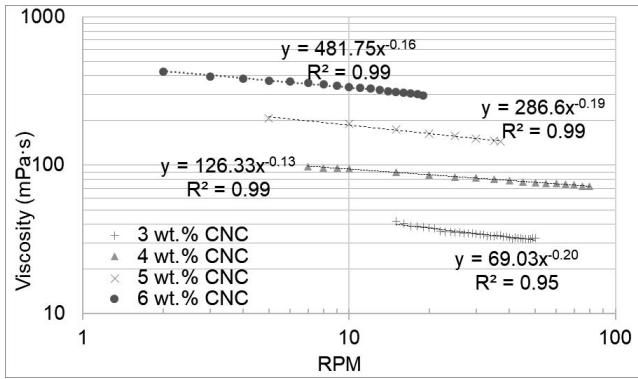
Figure 5.—The plot showing the relationship between apparent viscosity and spindle rotation speed.

Figure 6.—The relationship between the apparent viscosity and shear rate obtained from Method 2 (template method).

suspensions obviously showed that the CNC suspensions are not Newtonian liquids. Therefore, the primary readings of torque and rotational speed from the viscometer can be used as an approximation calculation using equations (3), (5), and (6) for the real shear rate and apparent viscosity. The equation for shear stress (eq. [1]) still applies for the real shear stress calculation for non-Newtonian liquid.

The second method (Method 2) calculating shear rate for the apparent viscosity measurement was employed to solve a differential equation (Krieger and Maron 1952, Krieger and Elrod 1953). The differential equation assumed that, in a laminar flow achieved during the measurement, the shear rate ($\dot\gamma$) for the liquid at the spindle surface is a function of the distance (r) from the spindle axis and the angular velocity (ω; Krieger and Maron 1952, Krieger and Elrod 1953, Middleman 1968, Sikdar and Oré 1979):

$$\dot\gamma = \frac{d\omega}{d(\ln r)} \tag{8}$$

Under steady rotation, the torque (M) in equation (1) is constant and the derivative of shear stress (τ) with respect to distance x (Krieger and Maron 1952, Krieger and Elrod 1953, Middleman 1968) gives the following:

$$d(\ln\tau) = -2d(\ln x) \tag{9}$$

Therefore, the shear rate at the spindle surface ($x = r$) can be calculated by (Middleman 1968)

$$\dot\gamma = 2\omega\frac{d(\ln\omega)}{d(\ln\tau)} \tag{10}$$

The shear stress (τ) and angular velocity can be calculated from equations (1) and (2) using the primary readings from the rotational viscometer. For the CNC suspension, which follows the power law flow model, a linear line can be obtained from a plot of ln ω against ln τ and the slope can be used in equation (10) for calculation of the shear rate. The apparent viscosity can then be obtained by dividing the shear stress by the shear rate. This method was developed by Rosen (Rosen 1971, 1972; Brookfield Engineering Laboratories 2017) and is called the template method. The relationship between the apparent viscosity and shear rate for the CNC suspensions obtained using this template method is shown in Figure 6. The initial observation indicated that the power law flow models of the CNC suspensions obtained from Method 2 are similar to those
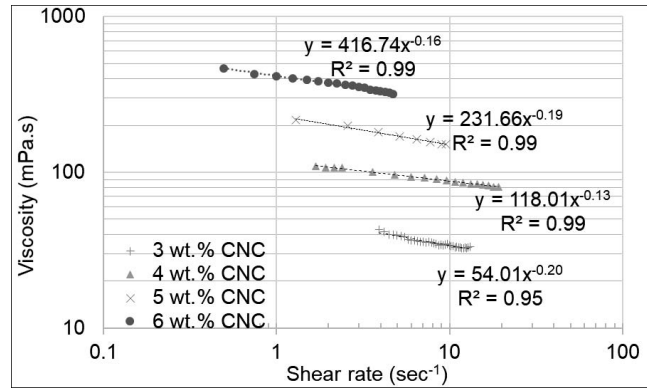
generated using Method 1 (Fig. 6). Compared with the models from Method 1, the same flow behavior indices n were obtained from Method 2 for the same CNC suspensions, but the consistency indices in the model obtained from Method 2 were different from those obtained from Method 1.

The third method (Method 3) in the literature used to calculate the apparent viscosity and shear rate was based on an empirical data treatment of the primary readings from the rotational viscometer, and two conversion factors used in the calculation were tabulated in the reference (Mitschka 1982). In this method, the shear stress for each measurement was calculated by multiplying torque reading in percentage with a parameter specific to each spindle,

$$\tau = k_{\alpha\tau}M \tag{11}$$

where $k_{\alpha\tau}$ is the parameter provided in the reference (Mitschka 1982) and the parameters are 0.035, 0.119, and 0.279 for spindles SP1, SP2, and SP3. For a fluid following the power law flow model, the plot of shear stress calculated from equation (11) versus spindle rotational speed (N in RPM) in a logarithm scale shows a linear relationship, and the slope of the linear line is simply equal to the flow behavior index n. For each flow index, a parameter of $k_{N\gamma}$ (n) can be identified from the table provided in the reference (Mitschka 1982). The shear rate is then calculated as

$$\dot\gamma = k_{N\gamma}(n)N \tag{12}$$

Following the procedures in the reference (Mitschka 1982), we calculated the viscosities and shear rate of the CNC suspensions. The plots of the apparent viscosity against shear rate obtained using this method showed similar shear thinning phenomena with the power law flow models, and the plots are not shown here.

The relationship between the apparent viscosity and shear rate for the CNC suspensions calculated from the three different treatment methods can all be modeled by the power law relationship and the model parameters are summarized in Table 1. For the same CNC suspension, the flow behavior indices n in the three power law flow models are the same. The flow behavior index is a measure of the liquid flow and determines the shear-thinning phenomena of the suspension (Mueller et al. 2009). For the same CNC suspension, the three different methods generated the same shear thinning observation. When the objective of the apparent viscosity

Table 1.—Summary of the power law parameters for the CNC suspensions.

Method	3 wt.%			4 wt.%			5 wt.%			6 wt.%		
	K	n	$\dot{\gamma}/N$	K	n	$\dot{\gamma}/N$	K	n	$\dot{\gamma}/N$	K	n	$\dot{\gamma}/N$
1	51	0.80	0.22	104	0.87	0.22	216	0.81	0.22	378	0.84	0.22
2	54	0.80	0.26	118	0.87	0.24	232	0.81	0.26	417	0.84	0.25
3	86	0.80	0.39	174	0.87	0.37	363	0.81	0.39	635	0.84	0.38

study is to understand the flow behavior and the shear thinning relationship (i.e., the viscosity changing with the shear rate), either one of the three methods can be applied. The plot of apparent viscosity against spindle rotation speed from the primary readings of the viscometer can also be used to obtain the shear thinning relationship for the CNC suspension (Fig. 5), and this plot works for non-Newtonian liquids to obtain the flow behavior index.

For the CNC suspensions at different concentrations, there is no pattern for the changing trend of the flow behavior indices. The CNC suspension at 3 wt.% has the smallest flow index of 0.80; and at 4 wt.%, the flow index is the largest (0.87). The CNC suspensions were obtained through suspending the high aspect ratios of CNC nanoparticles in rod shape in the Newtonian liquid of water, and the existence of the particle would affect the viscosity under the shear flow depending on the initial orientation and concentration of the particles (Powell 1991, Mueller et al. 2009). During the viscosity measurement, the shear flow introduced by the rotation of the spindle aligned the CNC particles in the flow direction. A greater shearing force applied at a higher spindle RPM provided more energy and an easier way to align the CNC particle, generating a lower viscosity and the shearing thinning phenomena (Shafiei-Sabet et al. 2012). At higher CNC concentrations, more work was needed to align more CNC particles, resulting in the need for greater torques (Fig. 4).

In the power law flow model, the viscosities of the CNC suspensions at different concentrations are most closely related to the consistency index ($K;$ Mueller et al. 2009), as shown in Table 1. Different consistency indices were obtained using different calculation methods for the same CNC suspension. Method 3 generated the largest consistency indices for all the CNC suspensions, followed by Method 2, and the consistency indices obtained from Method 1 are the lowest ones. The magnitude of the consistency index is cognate with the apparent viscosity of the suspension (Mueller et al. 2009). A higher consistency index indicates a higher apparent viscosity. The viscosity calculated using Method 3 showed a much higher number than that obtained from Method 2, which was slightly higher than that from Method 1. Method 1 calculated the viscosity based on an assumption that the liquid was Newtonian, and a potential error was introduced in this approximation calculation. Method 3 was an empirical data treatment process and could increase the statistical noise (data deviation from the true value) during the course of multiple data-fitting treatments. Method 2 (template method) was derived from an analytical evaluation with a one-time data-fitting treatment by extracting the slope of the plot of ln ω against ln τ (from eq. [10]) for the calculation of the shear rate. A high correlation coefficient of determination (R^2) for the plot of ln ω against ln τ can be demonstrated from Figure 4. Therefore, Method #2 is recommended for calculating the consistency index of the power law flow model for the CNC suspensions. Addition-

ally, we calculated the ratio of the shear rate to the spindle rotation speed (Table 1). For each method, we obtained a constant for the ratio of the shear rate to the spindle rotation speed. The slight difference in the constants in Methods 2 and 3 is caused by rounding up the number during calculation. All three calculation methods indicated that the shear rate of the CNC suspensions on the surface of the spindle changed linearly with the spindle angular velocity, which was the assumption for the calculation that there was no wall slip between the spindle surface and CNC suspension during spindle rotation. Different calculation methods generated different shear rates.

The consistency indices increased as the CNC concentrations increased from 3, 4, 5, to 6 wt.% (Table 1). A plot of the consistency index against the CNC suspension concentration in the logarithm scale produced a linear line for the three different methods (Fig. 7). The linear lines have a slope of approximately 3 with $R^2 = 0.99$. The relationship between the consistency index and the CNC suspension concentration indicated that the apparent viscosity of CNC suspension increased in a power law relationship with the weight concentration. To verify this relationship, we plotted the apparent viscosity of the CNC suspension against the suspension concentration at a specific shear rate. From Figures 3 and 5, it can be seen that there is a range of overlap on the shear rate calculated for the four CNC suspensions; and we selected a shear rate of 4 sec^{-1} located in this range to calculate the apparent viscosity for each suspension using equation (7) with the parameters obtained from Table 1. The relationships between the apparent viscosity and the CNC suspension concentration obtained from different calculation methods are shown in Figure 8, and linear relationships with slopes of 3 were observed for the plots in the logarithm scale. In addition, we measured all the apparent viscosities of CNC suspensions at 3, 4, 5, and 6
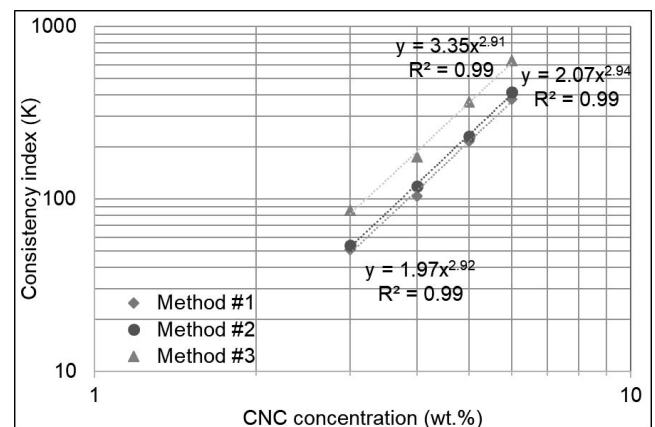

Figure 7.—The plot of consistency index of the power law model against CNC concentration.
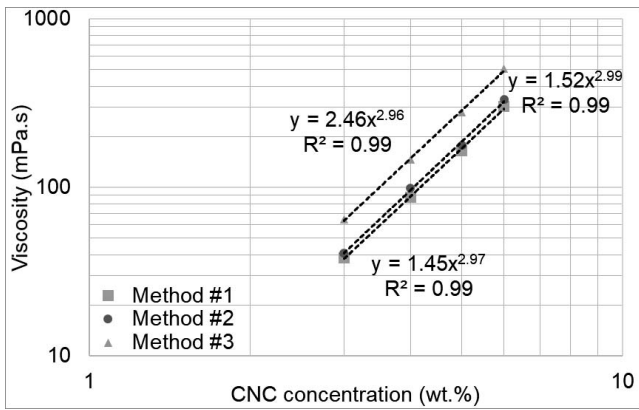
Figure 8.—The plot of viscosity of CNC suspension versus CNC concentrations at the shear rate of 4 sec^{-1}.

Figure 9.—The plots of the apparent viscosity of CNC suspension against shear rate measured using different spindles.

wt.% at the same spindle rotation speed of 15 RPM. The plot of apparent viscosity at the spindle rotation speed of 15 RPM versus the suspension concentrations generated the same linear relationship with the slope of 3 (not shown here). The relationship between apparent viscosity as plotted against the CNC suspension concentration is consistent with the relationship obtained for the consistency index versus the CNC suspension concentration (Fig. 7). In summary, the relationship between the viscosity of CNC suspension versus the suspension weight concentration (χ) in the measured concentration range can be expressed as

$$\eta \propto \chi^3 \qquad (13)$$

The rotational viscometer used in this study can quantify the viscosities of CNC suspensions at different concentrations. Power law flow models showing the shear thinning behaviors of the CNC suspensions were established with high coefficients of determination. The viscosity measurement method used in this study can be used in the quality control process characterizing the properties of different CNC suspensions. The model established through this method also can be used to predict the apparent viscosity of CNC suspensions at different shear rates and suspension concentrations. However, caution should be taken when extending the use of the power law flow model developed here to different CNC suspensions and large shear rate ranges because of large varieties of CNC sources and production processes (Bercea and Navard 2000, Buffa et al. 2019, Liao et al. 2020).

We also measured the viscosities of CNC suspensions at 5 and 6 wt.% using spindles SP2 and SP3. Method 3 described above was the only established method in the literature for calculating the shear rate for measurement results using spindles SP2 and SP3 (Mitschka 1982, Brookfield Engineering Laboratories 2017). The plots of apparent viscosities of the CNC suspensions versus shear rates are shown in Figure 9, with the measurement results using spindle SP1 included for comparison. Spindles SP2 and SP3 can widely extend the shear rate measurement capability using the rotational viscometer. Shear thinning behaviors were observed in the shear rate range measured in this study and power law flow models fitted well for all the measurement data. For the two CNC suspensions, viscosity measurement using different spindles showed overlapping shear rate range after calculation using Method 3 described
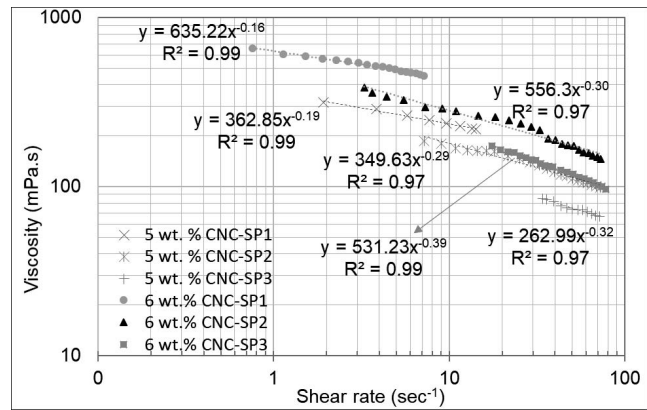
in the previous section (Fig. 9). However, under the same shear rate, the obtained viscosities were different for the same CNC suspension using the different spindles. The viscosities obtained for the CNC suspensions are highest using spindle SP1, followed by spindle SP2, and then by spindle SP3. For comparison of the viscosities of CNC suspensions, we do not recommend using different spindles even though the same shear rate was obtained using the calculation from Method 3. At the same time, the results indicated that Method 3 is not calculating the real shear rate for the rotational viscometer system. An additional data treatment method still must be developed for calculating the apparent viscosity and shear rate data when using spindles SP2 and SP3 in the rotational viscometer measurement.

The flow behavior indices in the power law flow models for the same CNC suspension are different when tested using different spindles. The flow behavior change of the CNC suspension at different shear rate ranges could be one of the reasons for this. Additionally, different spindle shapes (Fig. 2) used during rotation could apply different shear stress models to the suspension, resulting in different CNC particle alignments and, therefore, different flow behaviors. Spindle SP1 was a large cylindrical shape, whereas spindles SP2 and SP3 were disk-shaped. Rotation of spindle SP2 and SP3 would therefore generate different flow patterns than that of spindle SP1. Therefore, direct comparison among the results from different spindles would be inappropriate. The apparent viscosity data obtained from different spindles meant different shearing circumstances, which indicated that there is a high level of sensitivity when using a rotational viscometer to characterize the CNC suspensions.

Conclusions

We used a rotational viscometer successfully to quantify the rheological behavior of the CNC suspensions at concentrations of 3, 4, 5, and 6 wt. % at a certain shear rate range. We collected the primary readings of the rotational viscometer, including spindle rotation speed and torque, to evaluate the rheological properties of the CNC suspensions. We summarized three different methods of handling the primary reading data of a rotational viscometer from the literature and applied these to calculate the viscosity and shear rate of the CNC suspensions. We observed shear thinning behavior obeying the power law

flow model for all the CNC suspensions at the measured shear rate range. We critically analyzed differences among the calculation results from the different methods and recommend Method 2 (template method) for calculating the viscosity and shear rate for the CNC suspensions. In general, Method 2 is appropriate for viscosity calculation for a power law fluid. Method 1 can be used for rapid measurement of viscosity of Newtonian liquids with a direct viscosity reading. Method 3 needs to be used appropriately when spindles SP2 and SP3 are employed in the viscosity measurement, and Method 3 is the only method appropriate to handle the viscosity data for non-Newtonian liquids when spindles SP2 and SP3 are used with a rotational viscometer.

At different concentrations, the consistency and flow behavior indices in the power law flow models differed. With the same shear rate, higher concentration CNC suspension has a higher viscosity. A higher consistency index in the power law model was related to the higher viscosity of the suspension. The consistency index also can be directly obtained from the relationship between the apparent viscosity of the suspension and the spindle rotation speed. The apparent viscosity of the CNC suspension was also associated with the CNC concentration in a power law relationship.

When different spindles were used to measure viscosity of the CNC suspensions, different flow behaviors were generated in the same CNC suspension and direct comparison of the viscosity was inappropriate. This study indicated that a rotational viscometer can be used as a sensitive quality-control tool for characterizing the rheological properties of the CNC suspensions, and we made recommendations for calculating the viscosity and real shear rate of the CNC suspensions.

Acknowledgments

Literature Cited

Araki, J., M. Wada, S. Kuga, and T. Okano. 1998. Flow properties of microcrystalline cellulose suspension prepared by acid treatment of native cellulose. *Colloids Surf. A* 142:75–82.

Aulin, C., S. Ahola, P. Josefsson, T. Nishino, Y. Hirose, M. Osterberg, and L. Wagberg. 2009. Nanoscale cellulose films with different crystallinities and mesostructures—Their surface properties and interaction with water. *Langmuir* 25:7675–7685.

Bercea, M. and P. Navard. 2000. Shear dynamics of aqueous suspensions of cellulose whiskers. *Macromolecules* 33:6011–6016.

Brookfield Engineering Laboratories. 2017. More solutions to sticky problems: A guide to getting more from your Brookfield viscometer & rheometer. https://www.brookfieldengineering.com/-/media/ametekbrookfield/tech%20sheets/more%20solutions%202017.pdf?la=en. Accessed July 27, 2020.

Buffa, J. M., U. Casado, V. Mucci, and M. I. Aranguren. 2019. Cellulose nanocrystals in aqueous suspensions: Rheology of lyotropic chiral liquid crystals. *Cellulose* 26:2317–2332.

Chen, L. H., Q. Q. Wang, K. Hirth, C. Baez, U. P. Agarwal, and J. Y. Zhu. 2015. Tailoring the yield and characteristics of wood cellulose nanocrystals (CNC) using concentrated acid hydrolysis. *Cellulose* 22:1753–1762.

Eichhorn, S. J., A. Dufresne, M. Aranguren, N. E. Marcovich, J. R. Capadona, S. J. Rowan, C. Weder, W. Thielemans, M. Roman, S. Renneckar, W. Gindl, S. Veigel, J. Keckes, H. Yano, K. Abe, M. Nogi, A. N. Nakagaito, A. Mangalam, J. Simonsen, A. S. Benight, A. Bismarck, L. A. Berglund, and T. Peijs. 2010. Review: Current international research into cellulose nanofibres and nanocomposites. *J. Mater. Sci.* 45:1–33.

Habibi, Y., L. A. Lucia, and O. J. Rojas. 2010. Cellulose nanocrystals: Chemistry, self-assembly, and applications. *Chem. Rev.* 110:3479–3500.

Haŭgen, P. and M. A. Tung. 1976. Rheograms for non-law fluids using coaxial cylinder viscometers and a template method. *Can. Inst. Food Sci. Technol. J.* 9:98–104.

Hubbe, M. A., P. Tayeb, M. Joyce, P. Tyagi, M. Kehoe, K. Dimic-Misic, and L. Pal. 2017. Rheology of nanocellulose-rich aqueous suspensions: A review. *BioResources* 12:9556–9661.

Jeffrey, D. J. and A. Andreas. 1976. The rheological properties of suspensions of rigid particles. *AIChE J.* 22:417–432.

Krieger, I. M. 1968. Shear rate in the Couette viscometer. *Trans. Soc. Rheol.* 12:5–11.

Krieger, I. M., and H. Elrod. 1953. Direct determination of the flow curves of non-Newtonian fluids. II. Shearing rate in the concentric cylinder viscometer. *J. Appl. Phys.* 24:134–136.

Krieger, I. M. and S. H. Maron. 1952. Direct determination of the flow curves of non-Newtonian fluids. *J. Appl. Phys.* 23:147–149.

Li, M. C., Q. L. Wu, K. L. Song, S. Lee, Y. Qing, and Y. Q. Wu. 2015. Cellulose nanoparticles: Structure–morphology–rheology relationships. *ACS. Sustain. Chem. Eng.* 3:821–832.

Liao, J. S., K. A. Pham, and V. Breedveld. 2020. Rheological characterization and modeling of cellulose nanocrystal and TEMPO-oxidized cellulose nanofibril suspensions. *Cellulose* 27:3741–3757.

Lindström, T. 2017. Aspects on nanofibrillated cellulose (NFC) processing, rheology and NFC-film properties. *Curr. Opin. Colloid Interface Sci.* 29:68–75.

Middleman, S. 1968. The Flow of High Polymers: Continuum and Molecular Rheology. Interscience, New York, New York

Mitschka, P. 1982. Simple conversion of Brookfield RVT readings into viscosity functions. *Rheol. Acta* 21:207–209.

Moberg, T., K. Sahlin, K. Yao, S. Geng, G. Westman, Q. Zhou, K. Oksman, and M. Rigdahl. 2017. Rheological properties of nanocellulose suspensions: Effects of fibril/particle dimensions and surface characteristics. *Cellulose* 24:2499–2510.

Mueller, S., E. W. Llewellin, and H. M. Mader. 2009. The rheology of suspensions of solid particles. *Proc. R. Soc. A: Math. Phys. Eng. Sci.* 466:1201–1228.

Peng, Y., D. J. Gardner, and Y. S. Han. 2012. Drying cellulose nanofibrils: In search of a suitable method. *Cellulose* 19:91–102.

Powell, R. L. 1991. Rheology of suspensions of rodlike particle. *J. Stat. Phys.* 62:1073–1094.

Rånby, B. G. 1951. Fibrous macromolecular systems. Cellulose and muscle. The Colloidal properties of cellulose micelles. *Discus. Faraday Soc.* 11:158–164.

Revol, J. F., H. Bradford, J. Giasson, R. H. Marchessault, and D. G. Gray. 1992. Helicoidal self-ordering of cellulose microfibrils in aqueous suspension. *Int. J. Biol. Macromol.* 14:170–172.

Rosen, M. R. 1971. A rheogram template for power law fluids: Technique for characterizing the rheological properties of emulsions and polymer solutions. *J. Colloid. Interf. Sci.* 36:350–358.

Rosen, M. R. 1972. A rheogram template for power law fluids II. Rapid rheological characterization in a coaxial cylinder. *J. Colloid. Interf. Sci.* 30:413–417.

Shafiei-Sabet, S., W. Y. Hamad, and S. G. Hatzikiriakos. 2012. Rheology of nanocrystalline cellulose aqueous suspensions. *Langmuir* 28:17124–17133.

Sikdar, S. K. and F. Oré. 1979. Viscosity measurements of non-Newtonian slurry suspensions using rotating viscometers. *Ind. Eng. Chem. Prod. Res. Dev.* 18:722–726.

Urena-Benavides, E. E., G. Y. Ao, V. A. Davis, and C. L. Kitchens. 2011. Rheology and phase behavior of lyotropic cellulose nanocrystal suspensions. *Macromolecules* 44:8990–8998.

Williams, R. W. 1979. Determination of viscometric data from the Brookfield R.V.T. viscometer. *Rheol. Acta* 18:345–359.

Yang, T. M. T. and I. M. Krieger. 1978. Comparison of methods for calculating shear rates in coaxial viscometers. *J. Rheol.* 22:413–421.

Yasuda, K., T. Koshiba, and N. Mori. 2004. Effects of rheological property of coating liquid and withdrawal velocity on dip coating process in manufacturing of capsules. *J. Soc. Rheol.* 32 (2):85–90.